Published in final edited form as:
Sci Transl Med. 2012 April 11; 4(129): 129ra44. doi:10.1126/scitranslmed.3003249.

Model-Based Noninvasive Estimation of Intracranial Pressure from Cerebral Blood Flow Velocity and Arterial Pressure

Faisal M. Kashif[1], **George C. Verghese**[1], **Vera Novak**[2], **Marek Czosnyka**[3,4], and **Thomas Heldt**[1,*]

[1]Research Laboratory of Electronics, Massachusetts Institute of Technology, Cambridge, MA 02139 USA [2]Division of Gerontology, Beth Israel Deaconess Medical Center, Boston, MA 02215 USA [3]Department of Clinical Neurosciences, Addenbrooke's Hospital, University of Cambridge, Cambridge CB2 OSP UK [4]Institute of Electronic Systems, Warsaw University of Technology, Poland

Abstract

Intracranial pressure (ICP) is affected in many neurological conditions. Clinical measurement of pressure on the brain currently requires placing a probe in the cerebrospinal fluid compartment, the brain tissue, or other intracranial space. This invasiveness limits the measurement to critically ill patients. As ICP is also clinically important in conditions ranging from brain tumors and hydrocephalus to concussions, noninvasive determination of ICP would be desirable. Our model-based approach to continuous estimation and tracking of ICP uses routinely obtainable time-synchronized, noninvasive (or minimally invasive) measurements of peripheral arterial blood pressure and blood flow velocity in the middle cerebral artery (MCA), both at intra-heartbeat resolution. A physiological model of cerebrovascular dynamics provides mathematical constraints that relate the measured waveforms to ICP. Our algorithm produced patient-specific ICP estimates with no calibration or training. Using 35 hours of data from 37 patients with traumatic brain injury, we generated ICP estimates on 2,665 non-overlapping 60-beat data windows. Referenced against concurrently recorded invasive parenchymal ICP that varied over 100 mmHg across all records, our estimates achieved a mean error (bias) of 1.6 mmHg and standard deviation of error (SDE) of 7.6 mmHg. For the 1,673 data windows over 22 hours in which blood flow velocity recordings were available from both the left and right MCA, averaging the resulting bilateral ICP estimates reduced the bias to 1.5 mmHg and SDE to 5.9 mmHg. This accuracy is already comparable to that of some invasive ICP measurement methods in current clinical use.

*Correspondence: thomas@mit.edu.

Author contributions: F.M.K., G.C.V., T.H., and V.N. formulated the model. F.M.K., G.C.V, and T.H. developed the algorithm. M.C. collected and managed patient data. F.M.K. implemented and refined the algorithm and analyzed data. F.M.K., T.H., G.C.V, M.C., and V.N. evaluated validation results. F.M.K., T.H., and G.C.V. prepared the initial manuscript.

Competing interests: A patent application covering the estimation framework and associated algorithms was filed by MIT in September 2009 (following initial disclosure in September 2008), listing F.M.K., G.C.V., and T.H. as co-inventors. M.C. has a financial interest in the ICM+ software package for multimodal neuro-intensive care monitoring, for which a noninvasive ICP plug-in is commercially available (http://www.neurosurg.cam.ac.uk/pages/ICM/nICP.php).

Introduction

Intracranial pressure (ICP) is the hydrostatic pressure of the cerebrospinal fluid that surrounds the neural tissue and cerebral vasculature in the cranial cavity. Mean ICP for adults in the supine posture is normally 5–15 mmHg (1). However, ICP can rise dramatically in a variety of space-occupying intracranial pathologies, such as cerebral edema, intracranial hemorrhage, brain tumor, or acute hydrocephalus. The flow of oxygenated blood to the brain is driven by cerebral perfusion pressure (CPP), which is the difference between mean arterial pressure and ICP. An increase in ICP accordingly causes a decrease in cerebral blood flow (CBF) when compensatory mechanisms of cerebral autoregulation fail. Given the brain's sensitivity to even short disruptions in oxygen supply, it is not surprising that elevated ICP correlates with worsening of symptoms in patients with cerebrovascular injury, and can lead to serious consequences, including brain ischemia, neural damage, and brain death (2–4). Medical guidelines for traumatic brain injury (TBI), for example, require maintaining ICP below 20–25 mmHg and CPP above 60–70 mmHg (4–6).

The standard methods currently used for clinical monitoring of ICP to the desired tolerances are all invasive, requiring a hole to be drilled in the skull to advance a pressure probe or catheter into the brain parenchyma, or through the brain tissue into the ventricular space. With some sacrifice in measurement accuracy, ICP can also be monitored in the subarachnoid or subdural spaces, without entering the brain tissue, though still entailing penetration of the skull. All these approaches thus require neurosurgical expertise and carry the risk of infection and tissue damage. Assessment of spinal fluid pressure by lumbar puncture can also provide a spot estimate of ICP; however, this is not recommended when ICP is suspected to be high, because of the risk of brain herniation. Furthermore, a spot assessment cannot capture dynamic trends in ICP, which can by themselves be indicators of pathology.

The invasive nature of ICP measurement methods in current clinical practice has prevented more extensive availability of this neurological vital sign. Monitoring of ICP is mandated in patients with severe TBI and certain other serious conditions. However, if not for its invasiveness and risks, ICP measurements could benefit a much larger patient population, as assessment of ICP should ideally be indicated for diagnosis and monitoring in a wide range of neuropathologies. Candidate groups include patients with hemorrhagic or ischemic stroke, mild or moderate TBI (from sports, falls, or car accidents), altered mental status or cognitive/psychological disorders, hydrocephalus and implanted shunts, and brain tumors (7–9). Knowledge of ICP may also aid in establishing differential diagnoses in more benign conditions in which ICP measurements are not generally deemed necessary, such as headache, migraine, or visual problems. The development of a noninvasive ICP monitoring system with clinically acceptable accuracy is therefore warranted.

A variety of modalities has been explored for noninvasive ICP estimation (10) through measurement of related physiological variables; for instance, using ultrasound signals to measure cerebral blood flow velocity (CBFV) indices (11), skull vibrations (12), brain tissue resonance (13), or transcranial time-of-flight (14); venous ophthalmodynamometry (15);

optic nerve sheath diameter assessment (16); sensing tympanic membrane displacement (17); analyzing otoacoustic emissions (18); magnetic resonance imaging to estimate incremental intracranial compliance, and thereby ICP (19); and recordings of visual evoked potentials (20). The approach described by Ragauskas *et al.* (21) applied external pressure on the eyeball to balance the flow characteristics in the intra- and extracranial segments of the ophthalmic artery. The balance condition was then detected by a two-depth transcranial Doppler (TCD) ultrasound, and the corresponding external pressure taken as the estimate of ICP.

Some noninvasive ICP estimation methods feed simultaneous measurements of peripheral arterial blood pressure (ABP) along with TCD measurements of CBFV into multi-parameter mappings to generate the ICP estimate. Examples are mappings involving nested regressions (22), neural networks (23), or support-vector machines (24). The recording of ABP and CBFV waveforms in the clinical setting is quite routine; ABP measurement is already necessitated in a wide spectrum of critical care patients, and CBFV is the standard of care in patients with certain neurovascular pathologies. However, the large number of parameters and the lack of an underlying mechanistic model mean that such “black box” mappings can fail to adequately and robustly capture the relevant physiology.

Almost all the above noninvasive methods require calibration or tuning of parameters that relate the measured quantities to the ICP estimates. Such calibration or tuning typically involves the use of ICP measurements obtained invasively on the patient or from some reference population. Furthermore, training on a reference population causes the accuracy of the ICP estimates to depend on how well a particular patient is represented in the training set. As noted by Popovic and coauthors (10), after surveying nearly 30 noninvasive ICP methods patented over the last 25 years, none of the methods is sufficiently accurate to allow for routine clinical use. An additional factor in the way of clinical adoption for some of the proposed approaches is the difficulty or expense (hardware, computation, human resources) of the involved measurements. None of the previously proposed approaches to noninvasive ICP estimation has transitioned from the research setting to accepted clinical practice, though commercial products based on the methods in (17), (21) and (22) are available.

In this paper, we present a model-based approach to obtaining estimates of ICP on a beat-by-beat timescale, from noninvasive waveform measurements of CBFV and ABP. Our approach does not require patient-specific calibration, or training on a reference population. The associated computational burden is negligible, thereby allowing near-real-time estimation of ICP.

Results

Dynamic model and estimation algorithm

Detailed dynamic models of the cerebrovascular space (Fig. 1A) have been developed in the literature (25–27). We obtained a highly simplified model that focuses on the major intracranial compartments—brain tissue, cerebral vasculature, and cerebrospinal fluid (CSF) space—and the associated variables (Fig. 1B). The variables involved in the model are: ABP

at the level of the cerebral vasculature, CBF at the inlet of a major cerebral artery, and ICP. Our lumped model represents the relevant physiological mechanisms that couple these variables at the seconds-to-minutes time scale. The much slower processes of CSF production and absorption were neglected. The model also captures the fact that ICP, rather than systemic venous pressure, establishes the downstream pressure for cerebral perfusion. This is a consequence of the Starling resistor effect, resulting from the collapse of the cerebral veins owing to ICP being greater than venous pressure (27); it is also the reason that CPP is defined as the difference between mean ABP and ICP, rather than between mean ABP and systemic venous pressure.

Our model is conveniently specified by its electrical circuit analog (Fig. 1C), where pressures are represented by voltages, and flows by currents. The instantaneous ABP and CBF at time t are represented by the voltage $p_a(t)$ and the current $q(t)$, respectively. The effective resistance of the cerebral vasculature supplied by the MCA is represented by the resistor R, and the effective compliance of this cerebral vasculature and surrounding brain tissue is represented by the capacitor C. Our algorithm for estimation of ICP—with simultaneous estimation of R and C—resulted from requiring the model constraints to be satisfied as closely as possible by the obtained measurements, over an estimation window comprising the data associated with several consecutive beats, and under the assumption that ICP, R, and C are constant over that window.

For each estimation window, the algorithm generated one noninvasive ICP estimate (nICP), which can be considered an estimate of the mean ICP over the estimation window. The estimation window had to be long enough ($\gtrsim$5 beats) to allow some averaging of the data over multiple beats, with a corresponding attenuation of the effects of measurement noise, respiratory artifacts, and other such perturbations. However, the window also needed be short ($\lesssim$ 60 beats) compared to the timescales of significant transients in the underlying ICP.

The ABP in our model was arterial pressure at the MCA whereas our ABP measurement was made at the radial artery. These two arterial pressure waveforms undoubtedly differ in transit time from the heart and in pulse morphology; their mean values are close, however, provided measurements are taken with respect to a common reference. While there is no straightforward way to correct for morphological differences, our algorithm determines and applies an appropriate time shift to the measured radial artery ABP on the estimation window, in order to obtain a waveform that can serve as a plausible proxy for ABP at the MCA (see Methods).

Similarly, our measurements actually obtained CBFV rather than CBF. To the extent that the relation between these two can be approximated by just a scale factor, our method is able to use CBFV instead of CBF. This is because the particular structure of the model constraints causes the ICP estimate to be insensitive to any scaling of CBF, as long as this scaling remains constant over each estimation window (see Methods). The ICP estimate is therefore expected to be relatively insensitive to the cross-sectional area of the artery, the blood velocity profile across the vessel, and deviations of the insonation angle from its optimum, provided the combined effect of all these can indeed be captured (within each estimation window) by a single scale factor. When bilateral CBFV recordings are available, the ICP

estimates can be obtained from the left and right sides separately, though using a common ABP waveform.

Method validation in patients with traumatic brain injury

Validation of our method required a data set comprising simultaneous recordings of ABP, CBFV, and invasive ICP waveforms, all referenced to a common clock. Such carefully synchronized data are quite rare, but were available to us from comatose patients with severe closed-head injury admitted to neurological intensive care at Addenbrooke's Hospital, University of Cambridge, UK, between 1992 and 1997. Data acquisition was part of routine clinical care for daily assessment of cerebral autoregulation after TBI. In total, we used 45 records from 37 patients (some patients were examined more than once during their hospital stay) (table S1). These records for our blinded analysis were picked from the data archive to represent a wide range of ICP variations (0–100 mmHg) as well as substantial transients within a record (a change of up to 50 mmHg over the course of a few minutes).

The invasive ICP waveform was recorded from an indwelling parenchymal probe (Fig. 2A). Each patient record also contained simultaneously captured continuous waveforms of ABP from radial-artery catheterization and CBFV from TCD ultrasonography of the MCA, with bilateral recordings available for 30 of those records from 25 patients (Fig. 2B). The record lengths ran from 10 to 240 min. After excluding data segments in which either the ABP or CBFV waveform was dominated by significant noise or artifact, we were left with a total of approximately 35 hours of usable recorded data, which equaled more than 150,000 heartbeats. The patient population comprised 26 males and 11 females, with a median age of 25 years, and a median Glasgow Coma Scale (GCS) score of 5 (on a scale of 0–14), indicating severe TBI on admission. Further patient information, including the Glasgow Outcome Score (GOS) at six months after hospitalization, is provided in table S1.

In the blinded first stage of our protocol, the ABP and CBFV waveforms alone were used to construct our ICP estimates. The estimates were then compared against the invasively obtained ICP measurements in the second stage.

ICP estimation performance

In the results presented below, our ABP time-shift correction has been limited to picking a single time shift for each record (rather than for each estimation window), computed as optimal overall for the entire record. Furthermore, for uniformity, the results are presented for 60-beat estimation windows. Using non-overlapping windows of this size, we generated ICP estimates faster than once per minute, on average. The choice of a 60-beat window allowed averaging over several respiratory cycles. It is also possible to generate an estimate at each beat, even with a window comprising several beats, by "sliding" the estimation window one beat at a time. This corresponds to beat-by-beat estimation of ICP that has been averaged over the corresponding window. Prior to summarizing our estimation results across all the data in the 45 patient records (table S2), we present the results for four specific patients (Fig. 3). The results provide some orientation on the data and on the quality of the estimation results, and also illustrate the range of dynamic variations represented. The reported ICP is the beat-averaged ICP waveform, computed for every beat.

Among the more demanding tests of estimation performance is when the underlying ICP goes through substantial changes, as in the case of a “plateau wave,” in which ICP can spontaneously rise quite sharply to a level that is held for some time before returning to its previous baseline (28,29). One example (Fig. 3A) was recorded from a 23-year-old male (GCS = 7; patient record “AQ”). Our nICP estimates, computed in this instance on a sliding 60-beat window, closely tracked the transients in invasively measured, beat-averaged ICP. The root-mean-squared error (RMSE) over all beats was 5.1 mmHg, the mean error (bias) was 3.9 mmHg, and the standard deviation of error (SDE) was 3.2 mmHg. The RMSE, bias, and SDE are interrelated: the mean squared error (RMSE squared) is essentially the sum of the squared bias and the squared SDE. The RMSE is thus a useful aggregate measure of accuracy, whereas the SDE is a measure of precision or repeatability.

For all remaining results, the nICP estimates were computed on non-overlapping (rather than sliding) 60-beat windows. In computing the corresponding error statistics, these estimates were referenced against ICP averaged over the associated window.

Another patient, a 30-year-old male (GCS = 3; patient record “AK”), exhibited severe progressive intracranial hypertension (Fig. 3B). The nICP estimates closely tracked measured ICP, both during the initial 15 minutes when ICP held steady, as well as during the subsequent steady rise in measured ICP. The RMSE here was 6.0 mmHg, with a bias of −3.5 mmHg and an SDE of 5.0 mmHg.

A case in which our estimation algorithm fared less well involved two successive plateau waves in a 17-year-old male (GCS = 5; patient record “AO”) (Fig. 3C). The RMSE in this record was 10.2 mmHg, the bias was 3.9 mmHg, with an SDE of 9.4 mmHg. Although nICP closely tracked measured ICP in the initial part (<50 min) of this 4-hour recording, it deviated substantially from the measured ICP in portions of the remaining time. Nevertheless, the estimated ICP still captured the duration and amplitude of the second plateau wave as well.

It is also of interest to know how the estimation algorithm performs when ICP is closer to its normal range of 5 to 15 mmHg. In a 15-min recording from a 32-year-old female (GCS = 1; patient record “AR”), the nICP estimate tracked the measured ICP (Fig. 3D), with an RMSE of 5.4 mmHg, a bias of −4.8 mmHg and an SDE of 2.5 mmHg.

We summarize the estimation performance across all subjects in the form of Bland-Altman plots (30) of the estimation error, nICP−ICP, plotted against (nICP+ICP)/2 (Fig. 4). Here (as in Figs. 3B–D) nICP is the estimate computed over non-overlapping 60-beat windows and ICP denotes the average measured over the corresponding windows. Each plot was augmented by the corresponding error histogram, on which the plot of a Gaussian distribution of the same bias and SDE is superimposed for visual comparison.

In the 30 patient records in which bilateral CBFV recordings were available, we estimated ICP for each 60-beat window from the right- and left-sided CBFV signals independently, then averaged the resultant estimates to obtain nICP for that window. In the remaining 15 patient records in which only unilateral CBFV recordings were available, no such bilateral averaging could be performed. The error between nICP and measured ICP for all non-

overlapping, 60-beat windows, across all patients (a total of 2,665 estimates from non-overlapping data segments) showed a bias of 1.6 mmHg and SDE of 7.6 mmHg (Fig. 4A). Averaging these estimation results over ten consecutive 60-beat windows in each patient resulted in 287 comparisons of nICP with ICP, again employing disjoint data segments. The bias remained at 1.6 mmHg but the SDE dropped to 6.9 mmHg.

When we confined our analysis to only those 30 patient records for which we had bilateral CBFV recordings, and obtained nICP by averaging the ICP estimates from the right and left side, our results improved. Using 60-beat windows (1,673 total estimates), the bias and SDE were then 1.5 mmHg and 5.9 mmHg, respectively (Fig. 4B). Again averaging these estimation results over ten consecutive 60-beat windows (180 total comparisons), the bias remained at 1.5 mmHg, but the SDE dropped to 4.9 mmHg.

We also evaluated our estimates on a patient-record basis rather than data-window basis, comparing the average ICP and nICP values for each of the 45 patient records. The bias and SDE for this case were 0.9 mmHg and 6.5 mmHg, respectively (Fig. 4C).

The correlation coefficient between nICP and ICP, which is a measure of how well ICP can be predicted by an affine function of nICP, is often quoted in the literature on noninvasive ICP estimation. This correlation coefficient was determined to be 0.90 for the data obtained on the 2,665 non-overlapping estimation windows (Fig. 4A). The analysis in Bland and Altman (30) shows that a high correlation coefficient is indeed to be expected because the underlying ICP in our case varies over a range of 100 mmHg while nICP tracks it with a notably smaller SDE of 7.6 mmHg. Performing the same computation for the bilateral data set comprising 1,673 windows (Fig. 4B), the correlation coefficient dropped to 0.76 despite the smaller SDE of 5.9 mmHg, owing to the smaller range of underlying ICP variation (with only a few data points above 40 mmHg). A similar computation for the 45 estimates obtained on a patient-record basis (Fig. 4C) yielded a correlation coefficient of 0.92, reflecting the fact that the average ICP covers a range of about 75 mmHg across these records, while the corresponding SDE is under 6 mmHg.

Additional perspective on our results comes from examining the ability of the nICP estimates to correctly identify elevated ICP within our data set. A common threshold for treatment in TBI is an intracranial pressure of 20 mmHg (5), so we took ICP ≥ 20 mmHg as our definition of elevated ICP. For the 2,665 data pairs (Fig. 4A) and using an nICP of 20 mmHg as the threshold, we obtained a sensitivity of 83% and a specificity of 70% for detection of elevated ICP. A full receiver operating characteristic (ROC) was obtained by varying the nICP threshold from 0 mmHg to 100 mmHg (Fig. 5), with the definition of elevated ICP still being ICP ≥ 20 mmHg. This resulted in an area under the curve (AUC) of 0.83 for the ROC. We repeated this procedure on a patient-record basis. Using the earlier nICP threshold of 20 mmHg, the sensitivity and specificity were 90% and 80%, respectively. The ROC in this case (Fig. 5), again obtained by varying the nICP threshold, had an AUC of 0.88.

Referencing against ventricular ICP

Ideally our nICP validation should have been against *ventricular* ICP measurements, as these are regarded as the clinical standard. However, only intraparenchymal ICP measurements were available to us. Since parenchymal probes themselves show error against this ventricular standard, we derived what the errors in our validation results would be if nICP was compared against ventricular measurements.

If I_p is the parenchymal measurement and I_v is the ventricular measurement, then our validation error referenced against the parenchymal probe can be expressed as

$$\mathrm{nICP}-I_p=(\mathrm{nICP}-I_v)-(I_p-I_v), \quad (1)$$

where (nICP − I_v) is the estimation error our method would have if referenced to the ventricular standard, and (I_p − I_v) represents the error of the parenchymal probe relative to the ventricular measurement. Taking expected values and rearranging yields

$$bias(\mathrm{nICP}-I_v)=bias(\mathrm{nICP}-I_p)+bias(I_p-I_v). \quad (2)$$

Turning to variances, if the two error terms in parentheses in Equation 1 are uncorrelated (see Discussion), then the error variances are related by

$$var(\mathrm{nICP}-I_p)=var(\mathrm{nICP}-I_v)+var(I_p-I_v), \quad (3)$$

which can be rearranged as

$$var(\mathrm{nICP}-I_v)=var(\mathrm{nICP}-I_p)-var(I_p-I_v). \quad (4)$$

Discussion

Performance analysis and benchmarks

The accuracy measures for our noninvasive ICP estimation approach are competitive with all other noninvasive methods for ICP estimation reported in the literature to date (10), even when these others have to be calibrated or trained on invasive ICP measurements from the same patient or a collection of patients, for example (22–24). A good benchmark for noninvasive, calibration-free, patient-specific estimation of absolute ICP is the previously mentioned approach that applied external pressure on the eyeball while monitoring ophthalmic artery flow (21). Referenced to lumbar puncture with pressure covering a range of 3–37 mmHg, the method achieved a bias of 0.9 mmHg and SDE of 6.2 mmHg in a total of 57 comparisons. However, limiting factors were the data-acquisition time of 5–10 minutes per estimate and the intrusiveness of such an ocular procedure, both of which make the approach unsuited for continuous monitoring. Furthermore, the ability of this approach to estimate ICP levels higher than around 40 mmHg has yet to be established. In contrast, our approach can produce an estimate with just 5–60 beats of data (less than a minute), uses

data obtainable through standard clinical modalities, allows continuous monitoring, and has demonstrated good performance for ICP as high as 100 mmHg.

In establishing targets for the desired accuracy of noninvasive estimation methods, one should keep in mind that intra-beat and respiration-induced fluctuations of ICP are normally in the range of 2–3 mmHg, so it is unlikely that an RMSE smaller than 3 mmHg is required for ICP monitoring. It is also helpful to examine the accuracy of current invasive methods, and their mutual concordance. Ventricular and parenchymal pressure measurements are the primary approaches to invasive monitoring of ICP in clinical settings. The pressure as measured by a fluid-filled catheter located in a lateral ventricle remains the clinical gold standard against which other ICP measurement modalities ought to be evaluated; however, parenchymal and epidural probes are also often compared to one another.

Simultaneous measurement of ICP by a parenchymal probe and ventriculostomy showed a bias of −1.2 mmHg and an SDE of 3.4 mmHg in one study (31), although parenchymal probes have exhibited larger errors and drift over time in other studies (32–34). Simultaneous measurements of ICP by a parenchymal probe and an epidural probe have shown a bias of 4.3 mmHg, with an associated SDE of 8.5 mmHg (35). Subdural screws are deemed unreliable because of their relatively poor accuracy and tendency to underestimate high ICP, with median differences greater than 10 mmHg in 40–60% of comparisons against the ventricular catheter (36).

Given the above performance characteristics, our nICP estimation—with a bias under 2 mmHg and SDE under 6 mmHg—performs better than the invasive epidural and subdural measurements that are still used in current clinical practice. Furthermore, if intermittent ICP estimation suffices, temporal averaging of our nICP estimates reduces the RMSE. This was evident in the results presented for 10-window averaging, which preserved the bias at 1.5 mmHg and reduced the SDE from 5.9 to 4.9 mmHg in the case of 30 records with bilateral measurements.

As shown in Equation 2, the bias of our nICP relative to ventricular measurements will be the sum of its bias relative to parenchymal measurements and the bias of the parenchymal measurements relative to the ventricular standard. Thus the bias in our method relative to the ventricular standard might be greater or less than the bias obtained in our validation results, depending on the bias of the parenchymal probe. Similarly, Equation 4 shows that the precision of our estimates referenced to the ventricular standard could improve over the precision obtained in our validation results. The derivation of Equation 4 assumed that the errors between parenchymal and ventricular measurements are uncorrelated to the errors between our nICP and the same ventricular measurements. This assumption of uncorrelatedness is plausible because very different measurement modalities are involved. Our approach uses ABP and CBFV measurements along with a model, while the parenchymal probe involves a solid-state sensor in the brain parenchyma.

An expected use of a noninvasive ICP estimate would be for detection of elevated ICP. The potential of this approach is illustrated by our ROC analysis (Fig. 5), whose results are comparable with those reported, for example, in the setting of optic nerve sheath diameter

measurement for detection of elevated ICP (37). However, our patient population here was selected to display a large range of ICPs and is therefore not necessarily representative of the population in which such a test would primarily be applied. The performance on a population displaying a smaller range of ICP variation might not be as good.

Although the accuracy of a measurement method is certainly one of its most important performance characteristics, accuracy by itself may not be the primary performance measure in every clinical situation. For example, in particular pathologies, it might be adequate to track changes and trends in ICP, rather than track its absolute value; in this case, a bias may be of less concern, as long as it is relatively constant. Our nICP tracks plateau-wave changes as large as 50 mmHg over the course of 5 minutes (Fig. 3C), and in fact does so with low bias and SDE.

Features of our approach

Our approach uses routinely acquired signals, provides beat-by-beat and patient-specific estimates of ICP, does not require any training on population data, does not need calibration, and is applicable across a large range of ICP variations. Rather than relying on statistical associations, we leverage the underlying dynamic physiological relationships to generate patient-specific estimates of ICP.

The simple dynamic model of cerebrovascular dynamics in our framework is similar to the Windkessel model of systemic vascular dynamics (38). This model is widely used in the cardiovascular domain because it contains a small number of physiologically interpretable aggregate parameters that can be robustly estimated from the experimental data. Similar models have been used to some extent in the cerebrovascular setting (39, 40). A key difference of our model from these other cases is in pegging downstream pressure for cerebral blood flow as ICP rather than systemic venous pressure, which is crucial for estimating ICP from ABP and CBFV (41). More detailed models can be constructed (27), but it becomes fundamentally difficult to identify the more numerous parameters of such models from routine clinical measurements.

Simple static models relating available measurements to the physiological variables of interest underlie some commonly used clinical measurement modalities, such as pulse oximetry. The use of multivariable dynamic physiological models for similar purposes in clinical monitoring is still quite rare. However, extracting clinically meaningful information in real-time from multiple channels of high-resolution data virtually mandates the use of such physiologically based computational models. Our approach to noninvasive ICP estimation differs most fundamentally from previous attempts in its use of the salient dynamic physiological relationships among ABP, CBFV, and ICP.

Current limitations and future work

We have so far implemented our estimation algorithm in batch mode. However, the computations involved can be carried out in real-time. Apart from the pre-processing steps —such as noise filtering, beat-onset detection, and time-shift estimation—the computation of our ICP estimate entailed only the least-square-error solution of two linear systems of equations, each with one unknown (the compliance in one case, and the resistance in the

other). These are relatively trivial computations whose complexity varies linearly with the size of the estimation window. For example, our Matlab (The Mathworks) implementation took 0.13 s on a laptop (dual-core, 1.8 GHz) to compute continuous estimates for the 13-min patient record shown in Figure 3D, producing 13 nICP estimates in total. Additionally, as our algorithm provides one ICP estimate for each estimation window—without reference to data outside that window—it can be used for spot assessment or intermittent monitoring.

Further reductions in bias and SDE will be necessary to match the accuracy of parenchymal probes referenced against ventricular catheters. Because we extract detailed features of the ABP and CBFV waveform morphology on a beat-by-beat basis, the estimation performance directly depends on the signal quality (time and amplitude resolution, noise and artifact) of the acquired waveforms. Our validation tests were run on archived data collected over a multi-year period from 1992 to 1997, using varying equipment, personnel, and conditions. We anticipate that data collected on state-of-the-art instruments—and specifically with the requirements of our noninvasive ICP estimation algorithm in mind—will likely improve the accuracy of our method. For example, the sampling frequency of our validation data ranged from 20 to 70 Hz, whereas modern instrumentation provides samples at 125 Hz or higher.

The performance of our estimation routine critically depends on accurate time-alignment of the ABP and CBFV waveform features. We performed a carefully chosen time shift of the peripherally measured ABP waveform, to better approximate the required ABP at the location of the CBFV waveform. We have thus far only applied a single time shift to each entire patient record, although our method allows for estimation of a new time shift for each estimation window. It is possible that adaptive determination of the optimal time shift on a window-by-window basis will improve results. Also, a higher sampling frequency would allow finer determination of the time shift, as the offset is currently restricted to multiples of the sampling interval.

Our method should be tested on larger patient pools, with more diverse pathological characteristics than the group presented here, which comprises cases of severe closed-head injury. This validation can be pursued in patients with subarachnoid hemorrhage, hydrocephalus, or idiopathic intracranial hypertension, as the standard of care permits invasive measurement of ICP for these conditions. An additional task will be to validate the use of a strictly noninvasively obtained ABP waveform (42) in place of a measurement at the radial artery. Although the latter measurement is commonly available in the critical care setting, catheterization of a major artery will not be an option in many situations in which ICP estimates are desirable.

We have not made any use in this paper of the (arbitrarily scaled) estimates of cerebrovascular resistance and compliance, as seen from the MCA. These parameter estimates are obtained as adjuncts to our ICP estimates and associated CPP estimates, and determine the impedance of the local vascular bed. The dynamic response of the resistance and compliance estimates to changes in CPP may reflect the state of cerebrovascular autoregulation (43–45). Further work in this direction is warranted.

Overall, our results suggest that noninvasive, continuous, calibration-free and patient-specific estimation of ICP with clinically acceptable accuracy is feasible. Such technology has the potential to dramatically improve neuromonitoring in a variety of conditions in which ICP cannot be assessed currently.

Methods

Analysis of the anonymized data used in this study was approved by the Neurocritical Care Users' Committee at Addenbrooke's Hospital, and by MIT's Institutional Review Board.

Data pre-processing

In cases in which the input waveforms were contaminated with high-frequency noise, we applied a low-pass filter with a cut-off frequency at 16 Hz (chosen appropriately for the noise observed in our data). We up-sampled all data records to 125 Hz from their native sampling frequencies of 20 to 70 Hz. We subsequently applied a beat-onset detection algorithm (46) to mark the onset of each individual blood pressure wavelet. Finally, we reviewed the beat-onset annotations to delete double detections, insert missed detections, and exclude beats of low signal quality.

Estimation algorithm

The instantaneous cerebral perfusion pressure, $p_a(t)$ − ICP, in our circuit model (Fig. 1C) drives two components of flow, which together comprise the instantaneous CBF, $q(t)$. One component represents the main unidirectional flow through the cerebrovascular resistance, while the other component corresponds to the transient distention and contraction of the compliance. Thus

$$q(t)=\frac{p_a(t)-\mathrm{ICP}}{R}+C\frac{d(p_a(t)-\mathrm{ICP})}{dt} \quad (5)$$

We assumed ICP in each estimation window was essentially constant at its mean value within that window. This assumption corresponds to neglecting the effects of the intra-beat pulsations of ICP relative to those of pulsations in ABP, and neglecting the effects of slower variations in beat-averaged ICP over this estimation window, such as those induced by respiration. Similarly, despite the variations under autoregulation that are expected in R and C, we assumed that the effects of these variations were negligible over a short estimation window. These assumptions allowed us to set the derivative (or rate of change) of ICP to 0 in the estimation window, so the equation simplified to

$$q(t)=\frac{p_a(t)-ICP}{R}+C\frac{dp_a(t)}{dt} \quad (6)$$

Note that a scaled version of $q(t)$, say $\alpha q(t)$, satisfies

$$\alpha q(t)=\frac{p_a(t)-ICP}{R/\alpha}+\alpha C\frac{dp_a(t)}{dt} \quad (7)$$

which is identical to Equation 6, except that R and C have been scaled, with ICP and $p_a(t)$ left unchanged. This justifies our using CBFV instead of CBF, under the assumption that the two are related just by a scale factor that is constant over each estimation window. In our algorithm we set $\alpha = 1$, i.e., used CBFV as though it was CBF, with the result that our estimated R and C are in arbitrary units.

We used Equation 6 to develop a two-step estimation algorithm. Step I exploited the fact that the sharp transition in $p_a(t)$ during arterial systole induces a flow in the compliance that is large compared to that through the resistor, so the input flow $q(t)$ can be attributed primarily to the compliance branch in the model:

$$q(t) \approx C\frac{dp_a(t)}{dt} \quad (8)$$

Letting t_b and t_e indicate the beginning and end respectively of the systolic upstroke in $p_a(t)$, we can compute our estimate $\hat{C}$ of C by integrating Equation 8 over the transition period, and solving the resulting equation below for $\hat{C}$:

$$(p_a(t_e)-p_a(t_b))\,\hat{C}=\int_{t_b}^{t_e} q(t)dt \quad (9)$$

However, to mitigate the effects of noise, we obtained the least-square-error solution $\hat{C}$ of the system of equations that resulted from writing Equation 9 for each beat in the estimation window.

Step II used the result of Step I to estimate the flow through the resistance according to

$$\hat{q}_1(t)=q(t)-\hat{C}\frac{dp_a(t)}{dt} \quad (10)$$

Finite differencing was used to approximate the derivative. Expressing ICP in terms of $\hat{q}_1(t)$ using the relation

$$\mathrm{ICP}=p_a(t)-R\hat{q}_1(t) \quad (11)$$

allowed us to construct our estimate $\hat{R}$ of R using $\hat{q}_1(t)$ and $p_a(t)$ evaluated for two time instants t_1 and t_2 within a beat, again invoking our assumption that ICP is essentially constant during this beat (and throughout the estimation window). With this, $\hat{R}$ can be obtained by solving

$$(\hat{q}_1(t_2)-\hat{q}_1(t_1))\,\hat{R}=p_a(t_2)-p_a(t_1) \quad (12)$$

To reduce the sensitivity of this computation to the noise in $\hat{q_1}(t)$, we picked t_1 and t_2 to lie near the local minimum and maximum of the ABP pulse, respectively, and thereby maximize $\hat{q_1}(t_2) - \hat{q_1}(t_1)$. As with the compliance estimate, we then found the least-square-error solution $\hat{R}$ of the system of equations that resulted from writing Equation 12 for each beat of the estimation window.

Finally, re-writing Equation 11 in terms of beat-to-beat averages then gave the desired ICP estimate:

$$\hat{\mathrm{ICP}} = \overline{p_a(t)} - \hat{R}\overline{\hat{q}_1(t)} \quad (13)$$

where the overbars denote time-averages computed over the duration of one estimation window.

Time-shift correction of measured ABP

To estimate the time shift between radial ABP (ABP_{rad}) and ABP at the MCA (ABP_{mca}), we developed and applied two approaches motivated by the model in Equation 6. The first approach exploited the fact that near the inflection point of the ABP pulse during the systolic upstroke, the term $dp_a(t)/dt$ attains its maximum value. The value of the derivative rolls off to zero at the peak of systole or the end of diastole. Thus, within a given beat period, the maximum value of $q(t)$ must occur close to the time corresponding to the systolic inflection point of $p_a(t)$. The desired time shift is then taken to be the shift required to align the inflection point of the ABP_{rad} pulse with the maximum of the CBFV pulse.

The second approach was based on the observation that in the vicinity of the local extrema of the ABP pulse, the compliance-related term in Equation 6 can be ignored. The relationship between CBF and ABP_{mca} then becomes largely resistive and is determined by R and ICP only. Exploiting this insight, we developed a procedure to identify the local maxima and minima of ABP within each cardiac cycle, and determine through regression an affine relationship between CBFV and ABP_{rad} at a candidate time shift. The regression was repeated for various time shifts to find the one that yielded the smallest residual error, at which point the relation between CBFV and ABP was closest to being resistive.

We performed each time-shift calculation over a window of several consecutive beats, to mitigate the effects of noise and sampling. The median of the time shifts associated with all the windows in a record was used as the ABP time shift for the entire record. If the two time-shift estimation approaches yielded different values, we generated the corresponding nICP estimate for each and reported the average of the two estimates.

Supplementary Material

Refer to Web version on PubMed Central for supplementary material.

Acknowledgments

We are grateful to R. G. Mark of MIT for support and encouragement; I. T. Hwang for assisting in the analysis of the bilateral TCD data; and M. Kashif for guidance with the figures. Finally, this research had its origins in discussions at an American Institute of Mathematics workshop in Palo Alto, CA, October 2006, whose objectives

included discussion of “the methodological and computational framework for adapting complex mathematical models to clinical applications.”

Funding: F.M.K., G.C.V., and T.H. were supported in part by NIH R01 EB001659 and by the Center for Integration of Medicine and Innovative Technology, Boston. M.C. was supported by the National Institute of Health Research Biomedical Research Centre, Cambridge University Hospital Foundation Trust – Neurosciences Theme. V.N. was supported in part by NIH grants 4R37 AG2537-05 and 4P30 AG02871702.

References and Notes

1. Kandel, E.; Schwartz, J.; Jessell, T. Principles of Neural Science. 3. McGraw Hill; New York, NY: 2000. Appendix C
2. Miller J, Becker D, Ward J, Sullivan H, Adams W, Rosner M. Significance of intracranial hypertension in severe head injury. J Neurosurg. 1977; 47:503–516. [PubMed: 903804]
3. Levin H. Intracranial hypertension in relation to memory functioning during the first year after severe head injury. J Neurosurg. 1991; 28:196–200.
4. Steiner L, Andrews P. Monitoring the injured brain: ICP and CBF. Br J Anaesth. 2006; 97:26–38. [PubMed: 16698860]
5. The Brain Trauma Foundation. Guidelines for the management of severe traumatic brain injury, 3rd edition. J Neurotrauma. 2007; 24:S1–S106.
6. Hlatky R, Valadka A, Robertson C. Intracranial hypertension and cerebral ischemia after severe traumatic brain injury. Neurosurg Focus. 2003; 14:1–4.
7. Hoge C, McGurk D, Thomas J, Cox A, Engel C, Castro C. Mild traumatic brain injury in U.S. soldiers returning from Iraq. N Engl J Med. 2008; 358:453–463. [PubMed: 18234750]
8. Marmarou A. A review of progress in understanding and treatment of brain edema. Neurosurg Focus. 2007; 22:E1.
9. DeWitt D. Traumatic cerebral vascular injury: the effects of concussive brain injury on the cerebral vasculature. J Neurotrauma. 2003; 20:795–825. [PubMed: 14577860]
10. Popovic D, Khoo M, Lee S. Noninvasive monitoring of intracranial pressure. Recent Patents in Biomedical Engineering. 2009; 2:165–179.
11. Hanlo P, Peters R, Gooskens R, Heethaar R, Keunen R, van Huffelen A, Tulleken C, Willemse J. Monitoring intracranial dynamics by transcranial Doppler --- a new Doppler index: trans systolic time. Ultrasound Med and Bio. 1995; 21:613–621. [PubMed: 8525552]
12. Ueno T, Ballard R, Shuer L, Cantrell J, Yost W, Hargens A. Noninvasive measurement of pulsatile intracranial pressure using ultrasound. Acta Neurochirurgica Suppl. 1998; 71:66–69.
13. Michaeli D, Rappaport Z. Tissue resonance analysis; a novel method for noninvasive monitoring of intracranial pressure. J Neurosurg. 2002; 96:1132–1137. [PubMed: 12066918]
14. Ragauskas A, Daubaris G, Ragaisis V, Pektus V. Implementation of noninvasive brain physiological monitoring concepts. Med Eng Physics. 2003; 25:676–678.
15. Querfurth H, Lieberman P, Arms S, Mundell S, Bennett M, van Horne C. Opthalmodynamometry for ICP prediction and pilot test on Mt. Everest. BMC Neurol. 2010; 10:106. [PubMed: 21040572]
16. Borchert, M.; Lambert, J. Non-invasive method of measuring cerebrospinal fluid pressure. US patent application number. 09/021,966,. 1998.
17. Reid A, Marchbanks R, Bateman D, Martin A, Brightwell A, Pickard J. Mean intracranial pressure monitoring by a non-invasive audiological technique: a pilot study. J Neurol, Neurosurg Psychiatry. 1989; 52:610–612. [PubMed: 2732731]
18. Frank A, Alexiou C, Hulin P, Janssen T, Arnold W, Trappe A. Non-invasive measurement of intracranial pressure changes by otoacoustic emission (OAEs) – a report of preliminary data. Zentralbl Neurochir. 2000; 61:177–180. [PubMed: 11392287]
19. Alperin N, Lee S, Loth F, Raksin P, Lichtor T. MR-Intracranial pressure (ICP): a method to measure intracranial elastance and pressure noninvasively by means of MR imaging: baboon and human study. Radiology. 2000; 217:877–85. [PubMed: 11110957]
20. Zhao Y, Zhou J, Zhu G. Clinical experience with the noninvasive ICP monitoring system. Acta Neurochirurgica Suppl. 2005; 95:351–355.

21. Ragauskas A, Daubaris G, Dziugys A, Azelis V, Gedrimas V. Innovative non-invasive method for absolute intracranial pressure measurement without calibration. Acta Neurochirurgica Suppl. 2005; 95:357–361.
22. Schmidt B, Czosnyka M, Raabe A, Yahya H, Schwarze J, Sackerer D, Sander D, Klingelhöfer J. Adaptive noninvasive assessment of intracranial pressure and cerebral autoregulation. Stroke. 2003; 34:84–89. [PubMed: 12511755]
23. Mourad, P.; Mohr, B.; Kliot, M.; Frederickson, R. Systems and methods for determining intracranial pressure non-invasively and acoustic transducer assemblies for use in such systems. US patent. 7,547,283,. 2004.
24. Xu P, Kasprowicz M, Bergsneider M, Hu X. Improved noninvasive intracranial pressure assessment with nonlinear kernel regression. IEEE Trans Info Tech Biomed. 2010; 14:971–978.
25. Wakeland W, Goldstein B. A review of physiological simulation models of intracranial pressure dynamics. Compt Biol Med. 2008; 38:1024–1041.
26. Czosnyka M, Piechnik S, Richards H, Kirkpatrick P, Smielewski P, Pickard J. Contribution of mathematical modelling to the interpretation of bedside tests of cerebrovascular autoregulation. J Neurol, Neurosurg Psychiatry. 1997; 63:721–731. [PubMed: 9416805]
27. Ursino M, Lodi C. A simple mathematical model of the interaction between intracranial pressure and cerebral hemodynamics. J Appl Physiol. 1997; 82:1256–1269. [PubMed: 9104864]
28. Lundberg N. Continuous recording and control of ventricular fluid pressure in neurosurgical practice. Acta Psychiatrica et Neurologica Scandinavica. 1960; 36(Suppl 149):1–193.
29. Hayashi M, Handa Y, Kobayashi H, Kawano H, Ishii H, Hirose S. Plateau-wave phenomenon (I/II). Brain. 1991; 114:2681–2699. [PubMed: 1782538]
30. Bland J, Altman D. Statistical methods for assessing agreement between two methods of clinical measurement. Lancet. 1986; i:307–310. [PubMed: 2868172]
31. Koskinen LO, Olivecrona M. Clinical experience with the intraparenchymal intracranial pressure monitoring Codman MicroSensor system. Neurosurgery. 2005; 56:693–698. [PubMed: 15792507]
32. Morgalla M, Krasznai L, Dietz K, Mettenleiter H, Deininger M, Grote E. Methods of experimental and clinical assessment of the relative measurement accuracy of an intracranial pressure transducer. J Neurosurg. 2001; 95:529–532. [PubMed: 11565881]
33. Piper I, Barnes A, Smith D, Dunn L. The Camino intracranial pressure sensor: Is it optimal technology? An internal audit with a review of current intracranial pressure monitoring technologies. Neurosurg. 2001; 49:1158–1165.
34. Banister K, Chambers I, Siddique M, Fernandes H, Mendelow A. Intracranial pressure and clinical status: assessment of two intracranial pressure transducers. Physiol Meas. 2000; 21:473–479. [PubMed: 11110245]
35. Eide P, Sorteberg W. Simultaneous measurements of intracranial pressure parameters in the epidural space in in brain parenchyma in patients with hydrocephalus. J Neurosurg. 2010; 113:1317–1325. [PubMed: 20799859]
36. Mendelow A, Rowan J, Murray L, Kerr A. A clinical comparison of subdural screw pressure measurements with ventricular pressure. J Neurosurg. 1983; 58:45–50. [PubMed: 6847908]
37. Kimberly H, Shah S, Marill K, Noble V. Correlation of optic nerve sheath diameter with direct measurement of intracranial pressure. Acad Emerg Med. 2008; 15:201–204. [PubMed: 18275454]
38. Westerhof N, Lankhaar J, Westerhof B. The arterial Windkessel. Med Biol Eng Comput. 2009; 47:131–141. [PubMed: 18543011]
39. Zhu Y, Tseng B, Shibata S, Levine B, Zhang R. Increase in cerebrovascular impedance in older adults. J Appl Physiol. 2011; 111:376–381. [PubMed: 21617082]
40. Olufsen M, Nadim A, Lipsitz L. Dynamics of cerebral blood flow regulation explained using a lumped parameter model. J Appl Regulatory Integrative Computational Physiol. 2002; 282:R611–R622.
41. Kashif F, Heldt T, Verghese G. Model-based estimation of intracranial pressure and cerebrovascular autoregulation. Comput Cardiol. 2008; 35:369–372.
42. Parati G, Cadadei R, Gropelli A, di Rienzo M, Mancia G. Comparison of finger and intra-arterial blood pressure monitoring at rest and during laboratory testing. Hypertension. 1989; 13:647–655. [PubMed: 2500393]

43. Kashif, F. PhD thesis. Massachusetts Institute of Technology; Cambridge, MA: 2011. Modeling and estimation for non-invasive monitoring of intracranial pressure and cerebrovascular autoregulation.

44. Czosnyka M, Brady K, Reinhard M, Smielewski P, Steiner L. Monitoring of cerebrovascular autoregulation: facts, myths, and missing links. Neurocrit Care. 2009; 10:373–386. [PubMed: 19127448]

45. Novak V, Yang A, Lepicovsky L, Goldberger A, Lipsitz L, Peng C. Multimodal pressure-flow method to assess dynamics of cerebral autoregulation in stroke and hypertension. BioMedical Engineering Online. 2004; 3

46. Zong W, Heldt T, Moody G, Mark R. An open-source algorithm to detect the onset of arterial blood pressure pulses. Comput Cardiol. 2003; 30:259–262.

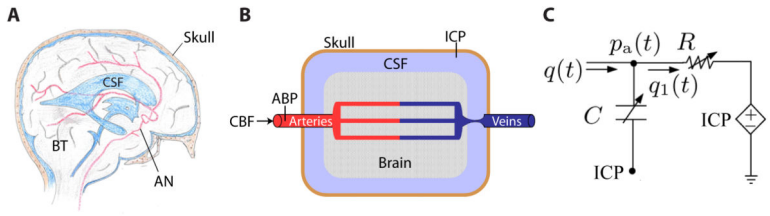

Fig 1.

Progressive abstraction of cerebrovascular physiology. (**A**) Relevant cerebrovascular anatomy: brain tissue (BT), cerebrospinal fluid (CSF), and cerebral arterial network (AN). (**B**) Schematic representation of the main cerebrovascular compartments and associated physiological variables: cerebral blood flow (CBF), arterial blood pressure (ABP), and intracranial pressure (ICP); the collapsed venous segment is also shown. (**C**) Lumped circuit-model representation of cerebrovascular physiology: cerebral blood flow $q(t)$, cerebral arteriovenous flow $q_1(t)$, and arterial blood pressure $p_a(t)$. ICP denotes both extra-luminal pressure and the effective downstream pressure for cerebral perfusion.

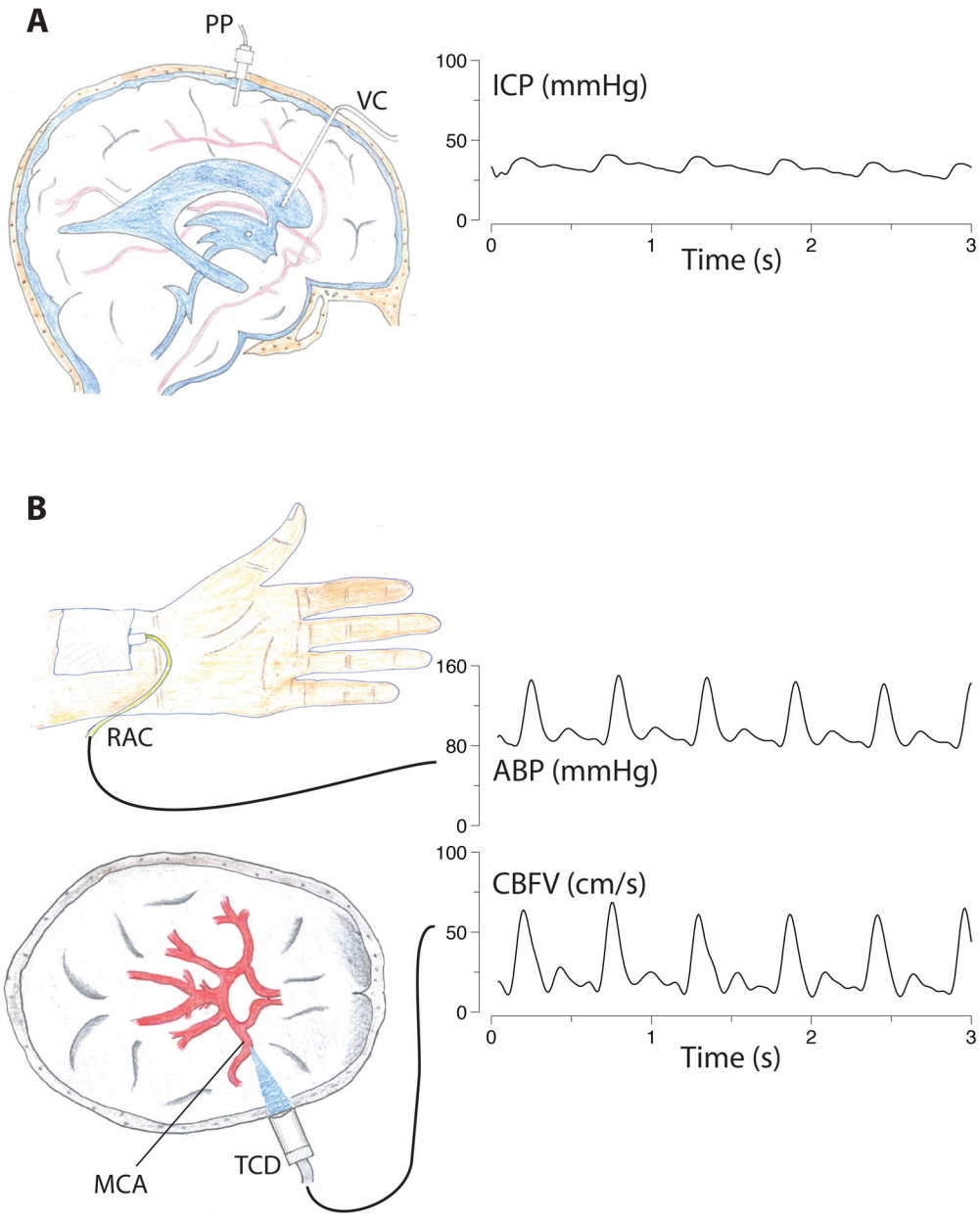

Fig. 2.

Schematic representation of data acquisition, showing representative intracranial pressure (ICP), arterial blood pressure (ABP), and cerebral blood flow velocity (CBFV) waveforms. (**A**) Possible direct, invasive recordings of ICP over time through a parenchymal probe (PP) or ventricular catheter (VC). (**B**) Invasive recording of ABP waveform through radial artery catheterization (RAC) and noninvasive recording of middle cerebral artery (MCA) blood flow velocity waveform by transcranial Doppler (TCD) ultrasonography, used together for noninvasive estimation of ICP.

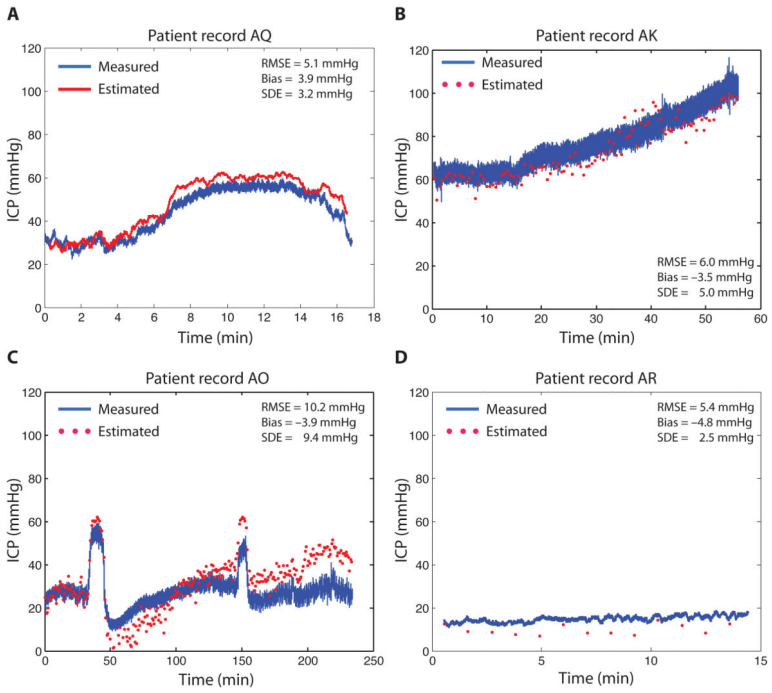

Fig. 3.

Comparison of measured and estimated ICP in four brain-injured patients. In panel A, ICP was estimated on a sliding 60-beat data window. In panels B–D, the estimates were obtained on 60-beat non-overlapping data windows. (**A**) Single plateau wave. (**B**) Severe progressive intracranial hypertension. (**C**) Two consecutive plateau waves. (**D**) Borderline normal ICP. All patient data are summarized in table S2.

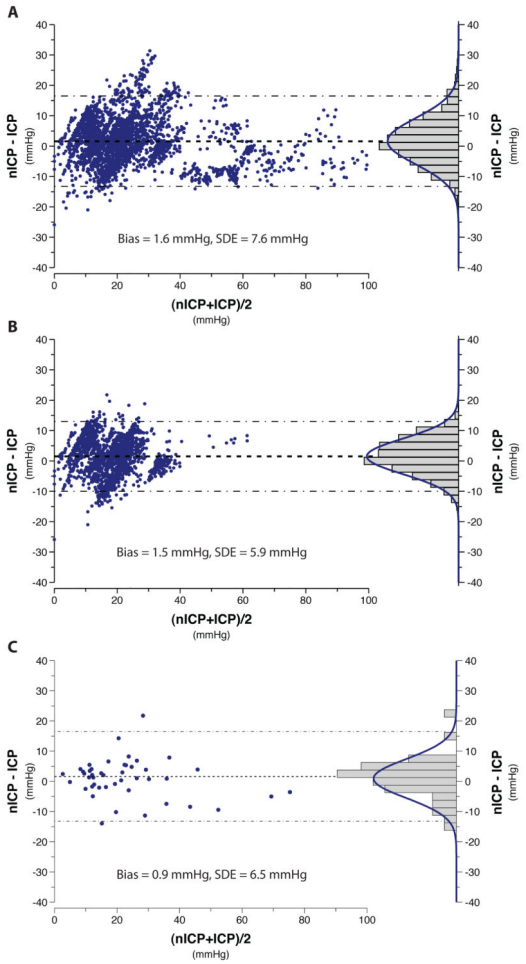

Fig. 4.

Bland-Altman plots of overall estimation performance. ICP is mean measured intracranial pressure and nICP is the noninvasive estimate, each computed on a 60-beat estimation window. (**A**) ICP and nICP on 2,665 non-overlapping windows from 45 patient records. (**B**) ICP and nICP on 1,673 non-overlapping windows from 30 records with bilateral CBFV recordings, where averaging of left and right estimates reduced the bias and SDE from (A). (**C**) ICP and nICP averaged across all windows in each of 45 patient records. For all three plots, the bias is shown as the dashed line and dash-dotted lines indicate the limits of agreement, computed as bias ± 2SDE.

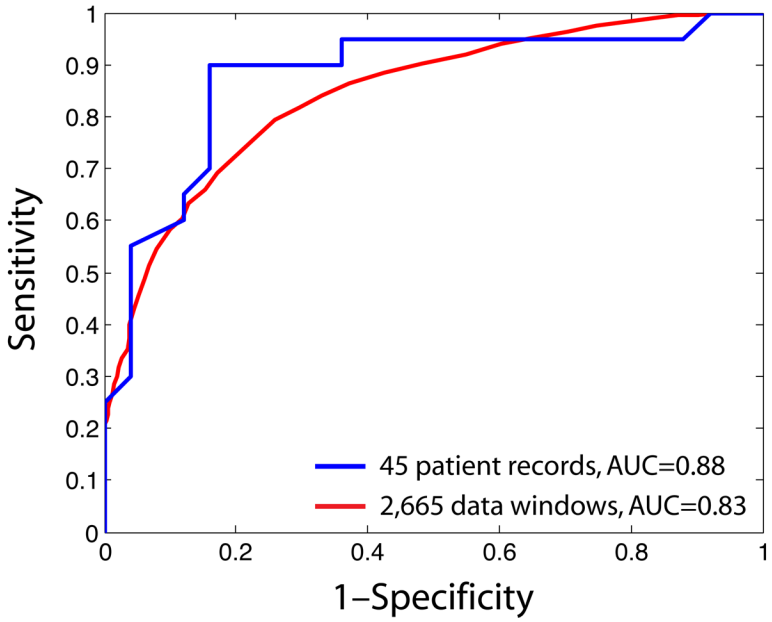

Fig. 5.

Receiver operating characteristics (ROC) for detection of intracranial hypertension, defined as ICP > 20 mmHg. One ROC was computed for all 2,665 nICP/ICP data pairs (red), and a second one for nICP/ICP data averaged across each of the 45 patient records (blue).